Coarse-grained model for gold nanocrystals with an organic capping layer

Philipp Schapotschnikow, René Pool, Thijs J.H. Vlugt

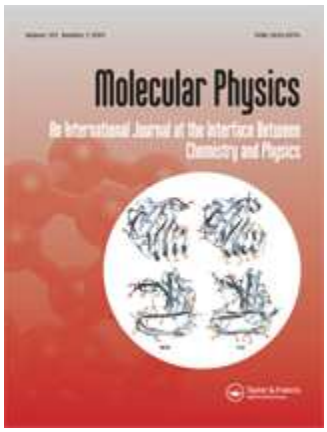

Coarse-grained model for gold nanocrystals with an organic capping layer

Journal:	*Molecular Physics*
Manuscript ID:	TMPH-2007-0274.R1
Manuscript Type:	Full Paper
Date Submitted by the Author:	09-Nov-2007
Complete List of Authors:	Schapotschnikow, Philipp Pool, René; Delft University of Technology, Process & Energy Laboratory Vlugt, Thijs; Delft University of Technology, Process & Energy Laboratory
Keywords:	nanocrystals, capping layer, molecular simulation, icosahedron
Note: The following files were submitted by the author for peer review, but cannot be converted to PDF. You must view these files (e.g. movies) online.	
paper_rev.tex bibdatabase_jpc_b.bib	

Coarse-grained model for gold nanocrystals with an organic capping layer

Philipp Schapotschnikow *, René Pool, Thijs J. H. Vlugt
Delft University of Technology
Process & Energy Laboratory
Leeghwaterstraat 44
2628CA Delft
The Netherlands

November 9, 2007

Abstract

We developed a coarse-grained interaction potential between icosahedral nanocrystals and united CH_x or SH atoms that interact via Lennard-Jones interactions. This interaction potential can be used to efficiently compute thermodynamic and structural properties of alkyl-thiol capping layers adsorbed on gold nanocrystals.

Keywords: nanocrystals, capping layer, molecular simulation, icosahedron

*p.z.schapotschnikow@tudelft.nl

1 Introduction

On microscopic length scales, the icosahedral structure is often observed. Many viruses, e.g. the Herpesvirus or the Poliovirus, take this shape.[1] Small clusters of up to 1600 atoms or molecules with Van der Waals attractions often form close-packed icosahedral structures at low temperature.[2] Although the structure of gold clusters of up to 5000 atoms is still subject to debate,[3–9] there is strong evidence that they have an icosahedral shape too.[5–9] Such metal or semiconductor clusters are called nanocrystals (NCs). They can be synthesized in a narrow size range by phase-transfer catalysis.[10,11] Surfactants such as alkyl thiols adsorb on the surface of a NC and form a capping layer, that hinders it from further growth and/or fusion with other particles. Moreover, they promote aggregation and self-assembly.[3] The 2D- and 3D-self-assembly of mono- and polydisperse gold NCs is a very exciting topic, since regular, periodic structures have been observed on a large scale.[12,13]

The fundamental interactions between NC building blocks that determine the formation of these superstructures cannot be easily accessed experimentally. Molecular simulation techniques such as Molecular Dynamics (MD) and Monte Carlo (MC) are the natural choice to study properties of these structures at the atomistic scale. For example, in the recent work,[14] a successful interplay between computer simulations and experiment shown that it is possible to predict and synthesize of new crystal structures from colloidal self-assembly. It would be very interesting to apply the same methodology to NCs.

Previous simulation studies on systems with one single gold NC capped with alkyl thiols have been carried out using a full atom description for NCs.[15–19] Due to high computational cost, only few studies investigated properties of systems with several NCs.[16,20,21] The NCs in those studies were relatively small (up to 140 atoms) compared to the ones typically used in assembly experiments.[12] Recent simulation studies[19,21] show, in addition, that the presence of solvent strongly influences the structure of capping layers. Our ultimate goal is to enable simulations of a large number of NCs with surfactant and solvent molecules at computationally affordable cost. However, due to the large size of such systems, a completely atomistic description for NC, capping layer and solvent would be computationally very expensive.

In this work, we develop a coarse-grained model for an icosahedral cluster of gold atoms interacting with point particles, yielding quantitatively the same properties as the full atom description. It is important to include the polyhedral shape in models of NCs whenever their facet size is larger than the distance between surfactants or of the same order as the surfactant length. For example, the separation between thiol headgroups on planar Au(111) surface is ≈ 5Å,[22] while the average end-to-end length of a dodecane-thiol surfactant at room temperature is ≈ 14Å.[15] For comparison, Au_{561} (diameter ≈ 27 Å) has an edge length of ≈ 14 Å. Therefore, a spherical interaction model will not be suitable for NCs of this size. Conversely, when facets become smaller than surfactants, the precise shape of the NC is of less importance and, therefore, smaller NCs such as Au_{140} (diameter ≈ 15Å) can be modeled spheres.[20]

In Ref.,[23] Hautman and Klein introduced an effective potential describing the interactions between surfactant atoms and an Au(111) surface. Their work can be interpreted as coarse-graining an extended surface into an interacting wall. The Hautman–Klein potential remains very popular for describing self-assembled monolayers of alkyl thiols on Au(111).[24–27] Our work can be considered as a 3D-generalization of the Hautman-Klein potential to icosahedral

clusters. In principle, the coarse-graining presented here can be applied to all kinds of faceted particles. To the best of our knowledge, this paper presents the first size- and shape-preserving interaction model for polyhedral particles.

2 Model

Consider a system consisting of a gold NC with an alkyl-thiol capping layer as in Fig. 1. We apply the united atom model to solvent and surfactant chain molecules, i.e. groups of atoms such as SH, CH_2 and CH_3 are combined into pseudoatoms. Pseudoatoms of the same molecule separated by three or less bonds interact with each other via bond stretching, bending and torsion potentials.[28] The non-bonded interactions and the interaction with gold in the full-atom representation are modeled by the Lennard-Jones (LJ) pair-potential

$$\phi_{\mathrm{LJ}}(r) = 4\,\epsilon\left[\left(\frac{\sigma}{r}\right)^{12} - \left(\frac{\sigma}{r}\right)^{6}\right] \tag{1}$$

with the potential well depth ϵ and the characteristic length σ. In our simulations the potential is truncated and shifted

$$\phi_{\mathrm{TS}}(r) = \begin{cases} \phi_{\mathrm{LJ}}(r) - \phi_{\mathrm{LJ}}(r_c) & r \le r_c \\ 0 & r > r_c \end{cases}, \tag{2}$$

with the cutoff radius $r_c = 12$Å, in line with our previous work[18,19]. Parameters for the carbon–carbon interactions are taken from Ref.,[28] for the thiol–thiol interaction from Ref.,[23] and for the gold–carbon and gold–thiol interactions from our previous work.[18,19] The lattice constant of gold is 4.08Å. For further details we refer the reader to Ref.[19]

We will exploit the high symmetry of the icosahedron (Ih) in our model. An Ih has 20 faces which are all equilateral triangles; at each of its 12 corners five faces meet, see Fig. 2(a). The 20 facet midpoints have the same distance to the center, which is called the in-radius R_{in}; the 12 corners also have equal distances to the center called the out-radius $R_{\mathrm{out}} \approx 1.26\,R_{\mathrm{in}}$. We will represent a NC as an Ih defined by the center of mass and 20 vectors connecting it to the facet midpoints. Although we develop and test our model for a rigid nanocrystal with 561 atoms (diameter ≈ 27Å, $R_{\mathrm{in}} = 10.6$Å), we will show that our coarse-grained model can also be applied to larger NCs.

3 Force field development

We consider a half-line starting from the NC-center. A certain part of this line lies inside the Ih. We denote its length by r_{ico} that obviously depends on the orientation of the half-line. The facet triangle pierced by this line is then the closest facet. If α is the angle between the half-line and the line connecting the center of the closest facet with the NC-center, then $r_{\mathrm{ico}} = R_{\mathrm{in}}/\cos\alpha$, see Fig. 2(b). We place a pseudo-atom at each point on this half-line and calculate its total interaction with the nanocrystal

$$U_{\mathrm{eff}}(r) = \sum_{i=1}^{N_{\mathrm{nano}}} \phi_{\mathrm{LJ}}(r_i) \tag{3}$$

with r being the distance to the NC-center, r_i the distance to the gold atom i and N_{nano} the number of atoms in the NC. We find that for all orientations we can fit $U_{\text{eff}}(r)$ with the same type of function:

$$U_{\text{eff}}(r) = \frac{5}{3}(2.5)^{\frac{2}{3}}\, U_{\text{min}} \left[\left(\frac{\tau}{r - r_{\text{ico}}} \right)^{10} - \left(\frac{\tau}{r - r_{\text{ico}}} \right)^{4} \right], \tag{4}$$

where U_{min} and τ determine the potential well depth and width respectively. The potential of Eq. (4) has a minimum at $r^* = r_{\text{ico}} + \tau\sqrt[6]{2.5}$ with the value $U(r^*) = -U_{\text{min}}$. Just as r_{ico} (Fig. 2(b)), the parameters τ and U_{min} (in principle) depend on the orientation of the half-line. Remarkably, we find that the value of τ differs by only 0.2Å for different orientations of the half-line and, therefore, it will be set constant in the remainder of this paper. Fig. 3(a) shows that the value of U_{min} is lowest in the direction of a facet center and highest in the direction of a corner, the difference is factor 3. This has also been observed for the effective interactions between an argon atom and a fullerene molecule.[29] The $10-4$ potential of Eq. (4) has the same asymptotic behavior as the coarse-grained model of Ref.,[20] where Au–CH_x interaction is modeled via $12-4$ potential. However, it is important to note that in that work the coarse-grained potential has a spherical symmetry (i.e. r_{ico}, τ and U_{min} are constant and do not depend on α), and hence the repulsive part of the potential (which results from the shape of the NC) is expected to be different.

We have calculated the effective interactions also for Au_{1415} (diameter $\approx$ 40Å), see Fig. 3(b). The size effect on the effective interaction is negligible, i.e. the parameters τ and U_{min} are the same for both NCs. Therefore, our coarse-grained model will also be applicable to all larger icosahedral NCs.

The icosahedral shape influences U_{min} significantly in the following way: at the facet midpoint a particle has more gold atoms in its neighborhood than on the edge, and hence more attractive contributions to the potential, see Fig. 2(a). This geometrical difference is expressed primarily by the value of the angle α. The well-depth U_{min} depends also on the atomistic structure of the surface. It is well-known that a thiol head prefers a hollow side between three gold atoms over a position on top of a gold atom.[22,30] This makes a convenient analytical expression for U_{min} impossible. The same problem arises when modeling extended surfaces, and the popular Hautman–Klein potential implicitly averages over the atomistic structure of bulk Au(111).

We calculate U_{eff} and U_{min} for half-lines going through points of the triangle limited by a facet center, edge center and a corner. Any point on the Ih–surface is equivalent to a point inside such a triangle by symmetry. We fit those minima to the function

$$U_{\text{min}} = U^C_{\text{min}} - \eta \sin^2 \alpha \tag{5}$$

with U^C_{min} being the well-depth at the facet center and η a constant fitting parameter, see Fig. 4(a). The term $\sin^2\alpha$ is chosen for computational simplicity. Parameters for different pseudoatoms are summarized in Table 1. Fig. 4(b) shows that, due to this averaging procedure, the effective potential is not reproduced as nicely as in Fig. 3(a) anymore. Nevertheless, the results of the next section show that our force field yields sufficiently accurate values for the energy. A convenient implementation of the potential defined by Eqs. (4) and (5) is described in the appendix.

It is important to note that our coarse-graining procedure is fundamentally different from the well-known approach by Hamaker.[31] An analytical expression for the attraction between spherical colloids was derived there. In that approach it is assumed that interaction centers are smeared out homogeneously over the object, and integrated the Van der Waals – attractions. In Ref.[32] the same integration was used for LJ interactions between spherical NCs and point particles. We tried this approach for our system. Along different half-lines, we integrated the LJ-potential $\phi_{\mathrm{LJ}}(r)$ over the Ih instead of the summation over the gold atoms in Eq. (3). The resulting effective interactions for SH are up to 1.5 times weaker than the ones obtained from Eq. (3); for CH_x both approaches yield similar results. Note that a typical distance between a thiol headgroup and the closest gold atom is approximately the same as the distance between two closest gold atoms (≈ 2.9Å),[30] and therefore SH can feel the discrete surface structure. Thus, the Hamaker approach is not always suitable for interactions between NCs and atoms.

4 Comparison of the coarse-grained and full atom models

As the main reason for coarse-graining the interactions between a NC and a united CH_x or SH atom is to reduce the computation time, we investigated the computational efficiency of the potential defined by Eqs. (4) and (5) and compared it to the full summation in Eq. (3). We found that an evaluation of the effective potential is on average 50 times faster than the explicit summation.

To obtain a quantitative justification of our coarse-graining procedure we compared average interaction energies. A large number of random positions at a fixed distance r from the NC-center was generated. For each of these positions, the interaction energy with a full-atom NC and the effective potential Eqs. (4) and (5) were calculated. A normal (unweighted) average as well as a Boltzmann average (i.e. weighted with $\exp(-U/k_BT)$ at $T = 300K$) over the values were taken. Relative energy differences of both averages between the two models were less than 20% close to the surface 14Å $\leq r \leq$ 16Å and less than 5% at large distances 18Å $\leq r \leq$ 21Å. The error is caused by the averaging over the atomistic structure, see Fig. 4 and is, therefore, inevitable. Note that the error becomes larger for $r \geq 20$Å when truncating the LJ potential in the full-atom model.

We performed MC simulations in the canonical ensemble (constant number of particles, volume and temperature) for NC fully covered with decane-thiol for both models. Several order parameters were compared at $T = 300K$: the radial distribution function (RDF) of surfactant centers of mass, the RDF between NC and surfactants, and the orientational distribution of surfactants. The latter is defined as follows. For each molecule, we defined the vector $\mathbf{b}$ that connects the first segment to the last. Furthermore, for each molecule, we calculated the vector $\mathbf{b}'$ that connects the NC center of mass to the molecule center of mass. We subsequently determined the distribution $P(\gamma)$ of the minimal angle $\gamma \in [0, \frac{\pi}{2}]$ between $\mathbf{b}$ and $\mathbf{b}'$. Low values of γ represent chains that are oriented perpendicular to the surface, whereas $\gamma \to \frac{\pi}{2}$ represent chains that are oriented parallel to the NC surface, see Fig. 5. The results are presented in Fig. 6. We conclude that the structure of surfactants is well described by the coarse-grained model.

For the same system, we have calculated the caloric curve, i.e. the potential energy as a function of temperature. The energies (in units of the Boltzmann constant k_B) computed using the effective potential are approximately $100000K$ (6%) lower than the ones computed using the full-atom model, see Fig. 7(a). Nevertheless, the shapes and slopes of the two curves are similar. The non-linear, noisy behavior of both curves around $280K$ (encircled in the figure) is due to the melting of the monolayer, see Figs. 1(a) and 1(b). At low temperatures, surfactant chains are aligned, while at high temperatures they are disordered. Experiments suggest that this transition should occur slightly below room temperature for decane-thiol.[33] Previous simulations yield transition temperature of $294K$ for dodecane-thiol on a larger NC.[15] We can conclude that our coarse-grained model is consistent with both experiments and full-atom simulations.

It is important to note, that in the full-atom model the LJ-potential was truncated and shifted. We applied a cutoff radius of 12Å. This yields a shift of each Au–S interaction (which has the largest contribution to the total energy) by $-1.3K$, i.e. $-1.3 \times 120 \times 561 = -87516K$ in total. We have added this number back, and obtained a very good agreement with the full atom model, see Fig. 7(a). Recall that the effective potential was fitted to the full LJ-potential; and no cutoff was applied in simulations with the coarse-grained interactions.

A rough estimate can be made for the efficiency of our coarse-grained potential. In the considered system there are 561 gold atoms and $11 \times 120 = 1320$ pseudoatoms (SH, CH_x). To calculate the total potential energy, 561×1320 NC–capping layer interactions and 1320×1320 interactions within the capping layer must be computed. Therefore, coarse-graining the NC–capping layer interactions can save $\approx 30\%$ of the computation time. This amount increases with larger NC size since the number of gold atoms scales with the volume while the number of surfactants scales with the surface area of the NC. The simulations with the effective potential were more than twice as fast than the full-atom ones. The main reason for this additional gain is the higher acceptance rate for trial moves in the coarse-grained model, yielding a faster equilibration and better sampling. Surface roughness causes lower acceptance probabilities in the full-atom model (see also Section 3).

We calculated the adsorption isotherm for propane-thiol in vacuum using the coarse-grained potential and compared it to the one calculated in our previous work using the full-atom model, see Fig. 7(b). They lie in the same range but the full-atom model isotherm shows a steeper curve. We have observed and explained this difference when comparing a full-atom Au(111) slab to an effective potential in our previous work.[19]

5 Conclusions

In this work, we have computed the total interaction energy between an icosahedral gold NC and Lennard-Jones particles. This interaction can be described by an effective 10-4 potential Eq. (4) with an isotropic (constant) value for τ. It turns out that the effective interaction is the same for all icosahedral Au–NCs with more than 500 atoms. The interaction strength ($U_{\min}$) is highly anisotropic as a result of the faceted surface. Averaging over the surface roughness, we obtained a coarse-grained interaction model Eqs. (4) and (5) that accurately describes interactions of united CH_x or SH atoms with a NC. This model was applied to a system with Au_{561} capped by decane-thiol and we found that the computed thermodynamic

properties hardly differ from those computed using the full atom model.

The force-field development presented in this work for icosahedral particles can be applied to any regular polyhedral shapes.

Acknowledgments

We thank Dr. Tim S. Jakubov for fruitful discussions. TJHV acknowledges the Netherlands Organization for Scientific Research (NWO-CW) for financial support through a VIDI grant.

A Computational details

Since the potential is developed for large-scale simulations, it should be as computationally cheap as possible. The first task is to find the closest facet center $\mathbf{f}$ for a given point $\mathbf{r}$. Assume that the NC-center is in the origin. We see that

$$|\mathbf{r}-\mathbf{f}|^2 = \langle \mathbf{r}-\mathbf{f}, \mathbf{r}-\mathbf{f}\rangle^2 = r^2 + R_{\text{in}}^2 - 2\langle \mathbf{r}, \mathbf{f}\rangle. \tag{6}$$

To find the closest facet center we identify the maximum of the dot product $\langle \mathbf{r}, \mathbf{f_i}\rangle$ where i runs over the 20 facets. We can use this immediately to check whether the point $\mathbf{r}$ lies inside the NC (in this case $\langle \mathbf{r}, \mathbf{f}\rangle \leq R_{\text{in}}^2$). Moreover, we obtain

$$\cos^2\alpha = \frac{\langle \mathbf{r}, \mathbf{f}\rangle^2}{r^2\, R_{\text{in}}^2}. \tag{7}$$

Explicit calculation of r and $\cos\alpha$ would involve an expensive (on some computers) evaluation of a square root, we avoid it as follows:

$$(r - r_{\text{ico}})^2 = r^2 + \frac{R_{\text{in}}^2}{\cos^2\alpha} - 2\frac{r^2 R_{\text{in}}^2}{\langle \mathbf{r}, \mathbf{f}\rangle}. \tag{8}$$

In a similar manner one can avoid square roots during force calculations in MD simulations.

References

1. Knipe, D.M., , *Fields Virology*, 5th ed. Lippincott Williams and Wilkins; Philadelphia, USA, 2006.

2. Echt, O.; Kandler, O.; Leisner, T.; Miehle, W.; Recknagel, E., *J. Chem. Soc. Faraday Trans.* **1990**, *86*, 2411-2415.

3. Whetten, R.L.; Shafigullin, M.N.; Khoury, J.T.; Schaaff, T.G.; Vezmar, I.; Alvarez, M.M.; Wilkinson, A., *Acc. Chem. Res.* **1999**, *32*, 397-406.

4. Cleveland, C.L.; Luedtke, W.D.; Landman, U., *Phys. Rev. B* **1998**, *60*, 5065-5077.

5. Wang, Y.; Teitel, S.; Dellago, C. *Chem. Phys. Lett.* **2004**, *394*, 257–261.

6. Marks, L.D., *Rep. Prog. Phys.* **1994**, *57*, 603-649.

7. Ascencio, J.A.; Gutiérrez-Wing, G.; Espinosa, M.E.; Martín, M.; Tehuacanero, S.; Zorrilla, C.; José-Ymacamán, M., *Surf. Sci.* **1998**, *396*, 349-368.

8. Koga, K.; Sugawara, K., *Surf. Sci.* **2003**, *529*, 23-35.

9. Chui, Y.H.; Grochola, G.; Snook, I.K.; Russo, S.P., *Phys. Rev. B* **2007**, *75*, 033404.

10. Brust, M.; Walker, M.; Bethel, D.; Schiffrin, D.J.; Whyman, R., *J. Chem. Soc., Chem. Commun.* **1994**, *7*, 801-802.

11. Murray, C.B.; Sun, S.; Gaschler, W.; Doyle, H.; Betley, T.A.; Kagan, C.R., *IBM J. Res. & Dev.* **2001**, *45*, 47-56.

12. Kiely, C.J.; Fink, J.; Brust, M.; Bethel, D.; Schiffrin, D.J., *Nature* **1998**, *396*, 444-446.

13. Fink, J.; Kiely, C.J.; Bethel, D.; Schiffrin, D.J., *Chem. Mater.* **1998**, *10*, 922-926.

14. Hynninen, A.P.; Thijssen J.H.J.; Vermolen E.C.M.; Dijkstra, M.; Van Blaaderen, A. , *Nature Mater.* **2007**, *6*, 202-205.

15. Luedtke, W.D.; Landman, U., *J. Phys. Chem. B* **1998**, *102*, 6566-6572.

16. Landman, U.; Luedtke, W.D., *Faraday Discuss.* **2004**, *125*, 1-22.

17. Lal, M.; Plummer, M.; Richmond N.J.; Smith, W., *J. Phys. Chem. B* **2004**, *108*, 6052-6061.

18. Schapotschnikow, P.; Pool, R.; Vlugt, T.J.H., *Comput. Phys. Commun.* **2007**, *177*, 154-157.

19. Pool, R.; Schapotschnikow, P.; Vlugt, T.J.H., *J. Phys. Chem. C.* **2007**, *111*, 10201-10212.

20. Tay, K.; Bresme, F., *Mol. Simulat.* **2005**, *31*, 515-526.

21. Patel, N.; Egorov, S.A., *J. Chem. Phys.* **2007**, *126*, 054706.

22. Ulman, A., *Chemical Reviews* **1996**, *96*, 1533-1554.

23. Hautman, J.; Klein, M., *J. Chem. Phys.* **1989**, *91*, 4994 - 5001.

24. Siepmann, J.I.; McDonald, I.R. *Mol. Phys.* **1992**, *75*, 255–259.

25. Siepmann, J.I.; McDonald, I.R. *Phys. Rev. Lett.* **1993**, *70*, 453–456.

26. Shevade, A.V.; Zhou, J.; Zin, M.T.; Jiang, S.Y., *Langmuir* **2001**, *17*, 7566-7572.

27. Vemparala, S.; Karki, B.B.; Kalia, R.K.; Nakano, A.; Vashishta, P., *J. Chem. Phys.* **2004**, *121*, 4323-4330.

28. Dubbeldam, D.; Calero, S.; Vlugt, T.J.H.; Krishna, R.; Maesen, T.L.M.; Smit, B., *J. Phys. Chem. B* **2004**, *108*, 12301-12313.

29. Jakubov, T.S.; Mainwaring, D.E., *Adsorption* **2007**, , in press.

30. Zhou, J.G.; Hagelberg, F., *Phys. Rev. Lett.* **2006**, *97*, 045505.

31. Hamaker, H.C., *Physica IV* **1937**, *10*, 1058-1072.

32. Rabani, E.; Egorov, S.A., *J. Phys. Chem. B* **2002**, *106*, 6771-6778.

33. Badia, A.; Lennox, B.; Reven, L., *Acc. Chem. Res.* **2000**, *33*, 475-481.

Table 1: Force field parameters for the coarse-grained interaction potential Eqs. (4) and (5).

	$U^C_{\min}/k_B$[K]	η/k_B[K]	τ[Å]
CH_3	1200	2500	2.9
CH_2	970	2020	2.9
SH	15500	25000	2.35

Figure 1: Gold NC capped with decane-thiol at two different temperatures. Gold atoms are represented by large dark spheres, thiol heads by small light spheres and carbon segments by lines. *(a)* The capping layer is melted ($T = 350K$). *(b)* The capping layer is frozen ($T = 250K$).

Figure 2: *(a)* Schematic representation of an icosahedral nanocrystal: atoms of the NC are represented by grey spheres, edges of the Ih by black lines. *(b)* A sketch of the effective potential calculation. Gold atoms are represented by large grey circles, a pseudo-atom (CH_x) by the black dot and the closest facet of the Ih by the bold vertical line. The half-line mentioned at the beginning of Section 3 connects the NC-center with CH_3. The bold dashed lines represent other facets. The distance between the pseudoatom (CH_3) and NC-center is r. Dashed arrows represent LJ interactions with the gold atoms, the sum of which is $U_{\text{eff}}(r)$ as in Eq. (3). The solid double-sided arrows indicate the in-radius R_{in} and the part of the half-line inside the Ih r_{ico}; the angle between them is α.

Figure 3: Effective interactions of pseudo-atoms CH_3 *(a)* and SH *(b)* with nanocrystals. *(a)* Effective Au_{561}—CH_3 interaction along half-lines through the midpoint, edge center and a corner of a facet (symbols); and fits to the $10-4$ potential of Eq. (4) (lines). For clarity, only every 15th symbol is displayed. Parameters τ and U_{min} result from fitting to the individual curves. *(b)* Effective Au_{561}—SH and Au_{1415}—SH interactions respectively, calculated in the direction of a facet midpoint and of a corner. Note that on the horizontal axis r_{ico} is subtracted. The pairs of lines corresponding to same directions coincide.

Figure 4: *(a)* The minima U_{min} of the effective interaction Eq. (4) as function of α for a large number of orientations for SH (represented by dots). The orientations are chosen uniformly from the triangle with corners at a facet center, at a corner and at an edge center; other orientations follow by symmetry of the Ih–surface. Circular patterns arise due to atomistic details of the surface. The fit to Eq. (5) with parameters from Table 1 is displayed by the solid line. The parameters are chosen in a way that low energies are better reproduced than the high ones.
(b) Effective Au_{561}—CH_3 interaction along half-lines through the midpoint, edge center and a corner of a facet (symbols), and according to Eq. (5) with parameters from Table 1 (lines), in contrast to Fig. 3(a) where the parameters were fitted to individual curves.

Figure 5: Definition of the angular orderparamter γ.

Figure 6: Orderparameters at $T = 300K$ calculated using the full atom model and the effective potential: *(a)* RDF of surfactants, *(b)* RDF between NC center and surfactants, *(c)* orientational distribution.

Figure 7: *(a)* Caloric curves for an Au_{561} capped with 120 decane-thiol molecules. The vertical offset is mainly due to cutoff in the full-atom model. The corrected curve is obtained by adding the cutoff energy back to the full-atom curve. *(b)* Adsorption isotherms for propane-thiol on Au_{561} in vacuum at $T = 300K$ calculated using the full-atom and the coarse-grained approach. On the horizontal axis is the density of the thiol in the ideal gas phase. On the vertical axis is the relative coverage. See Ref.[19] for more details.